bioRxiv preprint doi: https://doi.org/10.1101/2020.05.22.110775; this version posted May 22, 2020. The copyright holder for this preprint (which was not certified by peer review) is the author/funder. All rights reserved. No reuse allowed without permission.

Mycobacterium tuberculosis micro-diversity promotes intra-macrophagic persistence and antibiotic tolerance

Running title: Micro-diversity favors bacterial adaptive response

Charlotte Genestet[1,2*], Elisabeth Hodille[1,2], Alexia Barbry[1,2], Jean-Luc Berland[1,3], Jonathan Hoffman[1,3], Emilie Westeel[1,3], Jean-Baptiste Claude[3], Valentine Berti[2], Fabiola Bastian[4], Michel Guichardant[5], Samuel Venner[6], Florence Ader[1,7], Gérard Lina[1,2,8], Christophe Ginevra[1,2], Sylvain Goutelle[6,8,9], Oana Dumitrescu[1,2,8] on behalf of the Lyon TB study group

1. CIRI - Centre International de Recherche en Infectiologie, Ecole Normale Supérieure de Lyon, Université Claude Bernard Lyon-1, Inserm U1111, CNRS UMR5308, Lyon, 69007, France

2. Hospices Civils de Lyon, Institut des Agents Infectieux, Laboratoire de bactériologie, Lyon, 69317, cedex 04, France

3. Fondation Mérieux, Emerging Pathogens Laboratory, Lyon, 69007, France.

4. Plateforme DTAMB, CNRS, Université Lyon 1, Villeurbanne, 69622, France.

5. CarMeN laboratory, INSA Lyon, INSERM U1060, INRA U1397, Université Lyon 1, Villeurbanne, 69621, France.

6. Laboratoire de Biométrie et Biologie Évolutive, CNRS UMR 5558, Université Lyon 1, Villeurbanne, 69622, France

7. Hospices Civils de Lyon, Service des Maladies infectieuses et tropicales, Lyon, 69317, cedex 04, France.

8. Université Lyon 1, Facultés de Médecine et de Pharmacie de Lyon, Lyon, 69008, France

9. Hospices Civils de Lyon, Groupement Hospitalier Nord, Service pharmaceutique, 69322, Lyon, France

bioRxiv preprint doi: https://doi.org/10.1101/2020.05.22.110775; this version posted May 22, 2020. The copyright holder for this preprint (which was not certified by peer review) is the author/funder. All rights reserved. No reuse allowed without permission.

***Correspondence:** charlotte.genestet@gmail.com

Charlotte Genestet, PhD

Centre International de Recherche en Infectiologie, 7 rue Guillaume Paradin, 69003 Lyon, France

Tel: +33 (0)4 72 07 17 09

bioRxiv preprint doi: https://doi.org/10.1101/2020.05.22.110775; this version posted May 22, 2020. The copyright holder for this preprint (which was not certified by peer review) is the author/funder. All rights reserved. No reuse allowed without permission.

ABSTRACT

Mycobacterium tuberculosis (Mtb) genetic micro-diversity in clinical isolates may underline mycobacterial adaptive response during tuberculosis (TB) development and provide insights to anti-TB treatment response. Here, we investigated the genetic micro-diversity of persistent clinical Mtb isolates and its dynamics during controlled stress experiments chosen to mimic the course of TB disease. A minor variant characterized by a modified lipid profile, became enriched during stress experiments. The variant was found to be associated with drug-tolerance involving efflux pumps deregulation and with intracellular persistence subsequent to phagolysosome avoidance and autophagy decrease. Furthermore, pharmacological modeling predicted increased risk of treatment failure for isolates enriched in the former variant. Even under extreme experimental conditions, the diversity in variants was always maintained, suggesting a strong functional complementarity between variants of the Mtb bacterial population during disease dynamics. Such diversity may be responsible of Mtb adaptation to its host and play a role along the successive steps leading to multi-drug resistant TB. Altogether, our findings support the fact that Mtb micro-diversity should be further explored as a promising tool to detect patients at risk of poorly responding to anti-TB treatment, ultimately allowing improved and personalized TB management.

Key words

Mycobacterium tuberculosis; micro-diversity; whole genome sequencing; antibiotic tolerance; efflux pump; intra-macrophage persistence; phagolysosomal fusion; autophagic flux; apoptosis; inflammatory response

bioRxiv preprint doi: https://doi.org/10.1101/2020.05.22.110775; this version posted May 22, 2020. The copyright holder for this preprint (which was not certified by peer review) is the author/funder. All rights reserved. No reuse allowed without permission.

INTRODUCTION

Tuberculosis (TB) caused by *Mycobacterium tuberculosis* (Mtb) complex remains one of the most prevalent and deadly infectious diseases, responsible for 10 million cases and 1.45 million deaths worldwide in 2018 [1]. Among the reasons behind this dramatic situation stands the chronicity of Mtb infection, characterized by long periods of latency, linked to the ability of the tubercle bacilli to persist in the host tissues. TB disease therefore requires a long duration of antibiotic treatment to achieve sterilization of intracellular and intracavitary bacilli. Anti-TB drug resistance detection is mandatory upon TB diagnosis, as it is known to hamper treatment efficacy. However, persistent infections with delayed response to treatment may be observed without any *in vitro* proven antibiotic resistance. Hypothetically, pre-existing sub-populations enclosed within Mtb clinical isolates that are antibiotic tolerant could be responsible for such persistent infections [2, 3], but evidence of this is still lacking.

Since the introduction of next generation sequencing (NGS) enabling whole genome sequencing (WGS), WGS analysis performed on clinical Mtb isolates allowed to unmask the genetic particularities of Mtb sub-populations or variants. Minor variants are therefore frequently present within the diversity of Mtb population before treatment onset [4–9] and may also reveal during TB treatment. Some of these variants harbor drug-resistance mutations, whilst others carry SNP in loci involved in modulation of innate immunity and in Mtb cell envelop lipids [10–13]. Although the emergence of variants occurring in loci not directly related to drug-resistance is still poorly understood [14, 15], these could be the key to understanding early mechanisms leading to Mtb drug-resistance.

Genetic micro-diversity has been observed in other bacteria responsible for chronic infections, such as *Helicobacter pylori*, *Pseudomonas aeruginosa* and *Staphyloccocus aureus*, and has been linked to host-adaptation as well as disease outcome [16–18]. This raises the question of the influence of Mtb clinical isolates' micro-diversity on patients' response to anti-TB

bioRxiv preprint doi: https://doi.org/10.1101/2020.05.22.110775; this version posted May 22, 2020. The copyright holder for this preprint (which was not certified by peer review) is the author/funder. All rights reserved. No reuse allowed without permission.

treatment, beyond the canonical Mtb drug resistance phenomenon. We hypothesized that Mtb micro-diversity may be involved in bacilli persistence and in drug tolerance, both possibly favoring treatment failure. Thus, to better understand the evolution of Mtb micro-diversity during infection and treatment and its role in the pathophysiology of TB, we investigated variant composition and dynamics of persistent Mtb clinical isolates. Thereafter, we focused on 1 Mtb clinical isolate to capture its genetic diversity before and after controlled stress experiments chosen to mimic the course of TB disease. The identified variants stemmed from the initial clinical isolate were then assessed for their ability to tolerate the major anti-TB drugs and to persist during macrophage infection. Importantly, initial Mtb micro-diversity was found to be associated with both drug-tolerance and intra-cellular persistence and should thus be further considered to improve TB management and prevent treatment failure.

METHODS

Bacterial strains. Mtb strains used in this study were isolated from pulmonary specimens during routine care in the Lyon University Hospital, France. "Initial clones" IC_0 and IC_{100} were obtained by cloning of "initial isolate" (II). Clones were submitted to WGS to confirm the absence (IC_0) or presence (IC_{100}) of the variant of interest (C 3280555 G) and to confirm the absence of other mutations.

Antibiotics exposure using the BACTEC 960 system. Antibiotic exposure experiments were performed in Mycobacterial Growth Indicator Tube (MGIT) using the BACTEC 960 system (Becton Dickinson, Sparks, MD). Antibiotic solutions were added to MGIT at the required concentration and inoculated with 10^5 CFU/mL. Tolerance to antibiotics was also assessed in presence of efflux pump inhibitors reserpine (100µM, Sigma-Aldrich, Saint-Quentin-Fallavier,

bioRxiv preprint doi: https://doi.org/10.1101/2020.05.22.110775; this version posted May 22, 2020. The copyright holder for this preprint (which was not certified by peer review) is the author/funder. All rights reserved. No reuse allowed without permission.

France) and valinomycin (0.1 µM, Sigma-Aldrich). Results were expressed using MGIT time to positivity (TTP) system, reflecting the bacterial growth [19].

MIC Determination. Minimum inhibitory concentrations (MIC) were determined for rifampicin (RIF) and isoniazid (INH, Sigma-Aldrich) by a standard microdilution method as previously described [20].

Mtb RNA extraction and reverse transcription. Mycobacteria were incubated with RNAprotect Bacteria Reagent (Qiagen, Valencia, CA), lysed and Mtb total RNA was isolated by using RNeasy Plus mini kit according to the manufacturer's instruction (Qiagen). Reverse transcription was performed by using Reverse Transcription System according to the manufacturer's instruction (Promega, Fitchburg, USA).

Droplet digital PCR. ddPCR procedure was conducted using QX100 Droplet Digital PCR System (Bio-Rad, California, USA). Total reaction volume was 22 µL, containing 11 µL of 2X ddPCR Supermix for Probes (No dUTPs), 8.9 µL of template DNA, 10 U of HindIII restriction enzyme (GmbH) and 1.1 µL of a 20X primers-probes mix (ddPCR mutant assay) provided by Bio-Rad and guaranteed following MIQE guidelines. The sequence studied was CGACACCGTTCGTGACCTCATCGCCCGTTGGGAGCAGCGGGACGTGATGGCGCGC GAGGTG[G/C]CCGTCGACGTGGCGTCGCACTCGCCTCAAGTCGATCCGATACTCG ACGATTTGGCCGCGGC and the product was 70 bp. A no-template control and a positive control were used in every ddPCR batch. PCR amplification was conducted after droplet generation. Analysis were done with QuantaSoft Analysis Pro software version 1.0.596 (Bio-Rad). Positive droplets were counted and percentages of wild-type and mutant templates were calculated (% mutant =[(n mixed population/2)+n mutant]/total n amplified).

bioRxiv preprint doi: https://doi.org/10.1101/2020.05.22.110775; this version posted May 22, 2020. The copyright holder for this preprint (which was not certified by peer review) is the author/funder. All rights reserved. No reuse allowed without permission.

DNA extraction, targeted NGS and WGS. Genomic DNA was purified from cleared lysate using a QIAamp DNA mini Kit (Qiagen). For targeted NGS, PCR were performed using high fidelity DNA polymerase with primers indicated in Table S1. DNA libraries were prepared with Nextera XT kit (Illumina, San Diego, USA). Samples were sequenced on NextSeq or MiSeq system (Illumina) to produce 150 or 300 base-pair paired-end reads, as previously described [21].

Bioinformatic analysis of Illumina data. Reads were mapped with BOWTIE2 to the H37Rv reference genome (Genbank NC000962.2) and variant calling was made with SAMtools mpileup, as previously described [21]. A valid nucleotide variant was called if the position was covered by a depth of at least 10 reads and supported by a minimum threshold rate of 10%. Regions with repetitive or similar sequences were excluded, i.e. PE, PPE, PKS, PPS, ESX. The WGS reference genome coverage ranges 96.5% to 99.0%, with an average depth of coverage of 46x to 185x.

Sequences have been submitted to European Nucleotide Archive (ENA) under accession number PRJEB37306.

Apolar lipid extraction and analysis by GC-MS. Mycobacterial apolar lipids were extracted as previously described [22, 23], hydrolyzed with KOH 5% in methanol at 100°C for 90 min and then acidified. Fatty acids released were extracted with chloroform-ethanol (3:1). The extracted fatty acids from lower phase were derivatized with pentafluorobenzyl bromide (PFB) and analyzed in the negative ion mode by gas chromatography-mass spectrometry (GC-MS/MS Agilent HP7890B/7000C). The gas chromatograph was operated at the Functional Lipidomics platform, acknowledged by IBiSA (Infrastructure in Biology, Health and Agronomy).

bioRxiv preprint doi: https://doi.org/10.1101/2020.05.22.110775; this version posted May 22, 2020. The copyright holder for this preprint (which was not certified by peer review) is the author/funder. All rights reserved. No reuse allowed without permission.

Killing kinetics of RIF and INH alone and combination and mathematical modeling. *In vitro* experiments of the antibacterial effect of INH and RIF alone and in combination, as well as the mathematical modeling of the results were performed as described elsewhere [20].

Cell Culture and Infection protocol. U937 cells were differentiated with PMA and infected with bacterial suspension at a multiplicity of infection (MOI) of 10:1 (bacteria to cells). Invasiveness and intracellular multiplication were evaluated as described elsewhere [24].

Immunofluorescence and image acquisition. Infected cells were stained for confocal microscopy analysis, 6 h and 24 h post-infection (hpi), as described elsewhere [24]. For the study of autophagic flux, 3 h before staining, cells were incubated with chloroquine (Sigma) 40µM.

CCF-4 assay for translocation of Mtb in host cell cytosol. Infected cells were stained with 50 µM CCF4 (Invitrogen, Carlsbad, USA) in buffer containing anion transport inhibitor (Invitrogen) for 2 h at room temperature, then were washed and fixed with PFA 4% for 30min, as recommended by the manufacturer, before performing directly fluorescence acquisition [25, 26]. The results obtained were normalized on intracellular bacterial load.

Measurement of lactate dehydrogenase (LDH) in cell culture supernatants. LDH release of U937 cell culture supernatant was measured at 24 and 96 hpi by using the colorimetric kit (Roche, Mannheim, Germany) and following the manufacturer's instructions.

bioRxiv preprint doi: https://doi.org/10.1101/2020.05.22.110775; this version posted May 22, 2020. The copyright holder for this preprint (which was not certified by peer review) is the author/funder. All rights reserved. No reuse allowed without permission.

Quantitative determination of apoptosis. At 24 and 96 hpi, infected cells were stained for apoptosis detection with Annexin V FITC (Thermo Fisher Scientific Inc, Waltham, USA) for 15min at room temperature. After fixing with PFA 4% for 30min, cells were analyzed using fluorescent microscopy.

Infected macrophage RNA extraction. Total macrophage RNA was obtained from Mtb-infected cells at 24 hpi using the Trizol method as previously described [27] and total RNA was isolated with miRNeasy mini kit according to the manufacturer's instruction (Qiagen).

Transcriptomic analysis. Transcriptomic analysis was performed at ViroScan3D/ProfileXpert platform (www.viroscan3d.com). Briefly, RNA from each sample was quantified using Quantus HSRNA method (Promega) and qualified using Fragment analyzer HSRNA (AATI). After quality control, total RNA were submitted to polyA capture using NextFlex poly(A) Beads (PerkinElmer, Waltham, USA), then mRNA were submitted to library preparation using NextFlex Rapid Directional mRNA (PerkinElmer) and 100 ng input. As recommended by the ENCODE consortium ERCC RNA spike-In (Invitrogen) were added to samples in order to ensure reproducibility of the experiments. Single-read sequencing with 75 bp read length was performed on NextSeq 500 high output flowcell (Illumina). Mapped reads for each samples were counted and normalized using FPKM method [28]. Fold change between the different groups were calculated using median of groups and *p*-value of difference were calculated using t-test with equal variance without p-value correction in the R software. Population clustering analysis from transcriptomic data was conducted using principal component analysis (PCA) with the R package ade4 [29]. Heatmaps were performed thanks to Heatmapper [30], using average linkage clustering method and Pearson distance measurement method.

bioRxiv preprint doi: https://doi.org/10.1101/2020.05.22.110775; this version posted May 22, 2020. The copyright holder for this preprint (which was not certified by peer review) is the author/funder. All rights reserved. No reuse allowed without permission.

Quantitative real time RT-PCR (qRT-PCR). Differential expression of selected genes was determined by qRT-PCR using FastStart Essential DNA Green Master kit (Roche) on the LightCycler® Nano Instrument (Roche), according to the manufacturer's instruction. The cDNA was amplified with gene specific primers (Table S2 (Mtb primers) and S3 (human primers)). The transcripts of 16S RNA and glyceraldehyde phosphate dehydrogenase (GAPDH) were used to normalize the Ct values of the Mtb and human target genes respectively. Fold change in gene expression was calculated using the formula $2^{-\Delta\Delta Ct}$.

Cytokine production assay. Cell culture supernatants were screened at 6, 24 and 96 hpi for the presence of 27 human cytokines and chemokines using the Bio-Plex Pro Human Cytokine Standard 27-Plex kit (Bio-Rad Laboratory, Hercules, USA) on a FLEXMAP 3D® analyzer (Luminex, Austin, USA). Data were analyzed using Bio-Plex Manager software version 6.1 (Bio-Rad Laboratory).

Statistical analysis. Statistical analyses were performed with Graph Pad Prism 5. Data obtained from lipidomic analysis, RIF exposure experiments, variant frequency analysis by ddPCR, quantitative RT-PCR, intracellular CFU counting, macrophage cell death and cytokines and chemokines production were expressed as mean ± standard deviation (SD). Means were compared using One-Way ANOVA with Bonferroni's correction or t-test. Parameter values obtained from pharmacological models were given as point estimate [95% confidence interval (CI)]. Confocal microscopy data were expressed as median values [interquartile range (IQR)]. Results were compared by using Kruskal-Wallis analysis, using Dunn's Multiple Comparison Test. *$p<0.05$, ** $p<0.01$, *** $p<0.001$. $ Significantly different from condition without chloroquine; $ $p<0.05$, $$ $p<0.01$, $$$ $p<0.001$.

bioRxiv preprint doi: https://doi.org/10.1101/2020.05.22.110775; this version posted May 22, 2020. The copyright holder for this preprint (which was not certified by peer review) is the author/funder. All rights reserved. No reuse allowed without permission.

RESULTS

A minor variant of Mtb clinical isolate is selected in response to both rifampicin exposure and macrophage infection.

Sixteen clinical pan-susceptible strains isolated from the sputum of patients undergoing anti-TB treatment for 4 to 29 weeks were exposed for 4 weeks to rifampicin (RIF), *in vitro*, at 1xMinimum Inhibitory Concentration (MIC) to investigate the emergence of variants. A total of 32 SNPs emerging in 12 out of 16 Mtb strains after RIF exposure were identified (Table S4). Following RIF exposure, one of these 12 isolates showed dramatic increase of the frequency of a single variant, harboring 1 non-synonymous SNP C 3280555 G, in a locus involved in cell wall and cell processes (Rv2940c *mas*, Table S1). To decipher the dynamics of the variant composition of this clinical isolate we first performed WGS on 20 grown colonies plated before *in vitro* RIF exposure. Apart from the predominant clone, 4 variants were identified and their presence in the initial isolate was confirmed by targeted next generation sequencing (NGS), at frequencies between 0.5% and 9% (Fig. 1A). Six loci differed amongst the variants, with a maximum pairwise distance of 4 SNPs. Independently from RIF exposure, the initial isolate was submitted to 7 days of macrophage infection. Interestingly, NGS analysis of these two final isolates found that the C 3280555 G variant was the most enriched during both RIF exposure (from 1.5% to 45%) and macrophage infection (from 1.5% to 74%), whilst the relative frequency of the others 3 variants varied within a range of 10% (Fig. 1A).

To further study the emerging C 3280555 G variant, 5 strains containing the C 3280555 G variant at various frequencies were compared: the initial clinical isolate named “initial isolate” (II); 2 “evolved isolates” (EI) enriched in the C 3280555 G variant at a mean frequency of either 40% (EI_{40}) after RIF exposure or 80% (EI_{80}) after macrophage infection; 1 clone representing the predominant clone of the II, not carrying the C 3280555 G polymorphism (Initial Clone, IC_0); and 1 clone of the II carrying the fixed C 3280555 G polymorphism (IC_{100}; Fig. 1B).

bioRxiv preprint doi: https://doi.org/10.1101/2020.05.22.110775; this version posted May 22, 2020. The copyright holder for this preprint (which was not certified by peer review) is the author/funder. All rights reserved. No reuse allowed without permission.

The C 3280555 G harboring variant overexpresses mycocerosates and more particularly the tetramethyl-branched components of mycocerosates.

The SNP C 3280555 G results in an amino-acid change, A721P, of mycocerosic acid synthase (Mas, Rv2940c). It is located in Mas acyltransferase domain, involved in multimethylated mycocerosates synthesis by iterative condensation with methyl-malonyl-CoA units [31, 32]. Mycocerosates are components of the phthiocerol dimycocerosate (PDIM) family of lipids of Mtb, strongly involved in host-pathogen interaction. Because the mycocerosate components are expected to be altered in the C 3280555 G variant, the lipid profile of IC_{100} and IC_0 and a half-half mixture (50:50) was explored, focusing on the production of the 4 main components of mycocerosates (Fig. 2A): the two trimethyl-branched, C27 and C29, and the two tetramethyl-branched, C30 and C32 [22, 33]. When comparing to IC_0, IC_{100} profile showed significantly lower trimethyl-branched C27 component (11.4% ± 2.2%) than tetramethyl-branched C30 component (80.1% ± 2.4%; Fig. 2B), consistent with a higher affinity of Mas enzyme for methyl-malonyl-CoA, to promote tretramethyl mycocerosate synthesis in IC_{100}. Moreover, the relative proportion of mycocerosates produced by IC_{100} was approximately twice as high compared to IC_0 (Fig. 2C). Given this lipid profile, the variant is called hereafter the 4MBE (tetra-methyl branched enriched) variant.

The 4MBE variant is tolerant to RIF alone and in combination with isoniazid.

As micro-diversity patterns changed upon RIF exposure, the susceptibility of the 4MBE variant to this drug was explored. Although there were no significant difference regarding the MIC values (Table S5), the tolerance of the 4MBE variant to sub-MIC doses of RIF was investigated. The kinetics of the bacterial growth explored by the time to positivity (TTP) approach, revealed a significantly shorter TTP for IC_{100}, EI_{80}, and EI_{40} (from 6.9 to 9.7 days) compared to II (15.6

bioRxiv preprint doi: https://doi.org/10.1101/2020.05.22.110775; this version posted May 22, 2020. The copyright holder for this preprint (which was not certified by peer review) is the author/funder. All rights reserved. No reuse allowed without permission.

± 1.6 days) upon antibiotic treatment with 1xMIC of RIF (Fig. 3A). Controlled bacterial assembly experiments, mixing IC_0 and IC_{100} at various ratios, yielded similar results (Fig. S1A). Thus TTP values decreased as 4MBE variant frequency increased in the starting inoculum, suggesting a better ability of the 4MBE variant to persist upon RIF exposure.

To further explore RIF tolerance of the 4MBE variant, concentration-effect experiments were performed, and results yielded were then implemented in a pharmacological efficacy prediction model. There was a decrease in RIF susceptibility for EI_{40}, EI_{80}, and IC_{100} at sub-MIC doses (Fig. 3B). EI_{40}, EI_{80}, and IC_{100} exhibited higher EC_{50} values (from 2.3 to 5.9) than II (1.0, 95% CI [0.6; 1.6]), suggesting a lower potency of this antibiotic on 4MBE variant. Regarding IC_{100}, there was a significant decrease in the Hill coefficient value (0.61 [0.49; 0.74]) compared to EI40 (0.96 [0.79; 1.13]) and EI_{80} (0.89 [0.72; 1.06]), indicating also a better tolerance to supra-MIC concentrations of RIF (Table S6). Overall, these results indicate that 4MBE variant is tolerant to sub-MIC doses of RIF compared to II, despite the absence of canonical RIF resistance.

As RIF is part of a complex regimen during TB treatment, the antibacterial effect of the combination of both first-line anti-TB drugs (isoniazid (INH) and RIF) was investigated on IC_0 and IC_{100} (Fig. 3C). The Minto model described the combined antibacterial effect very well, R^2 values ≥ 0.90 and low bias and imprecision values. Importantly, the interaction parameter β_{U50} was significantly greater than 0 for IC_0 (1.43 [0.94; 1.91]), which means that the combined effect of INH and RIF was synergistic. Conversely, it was not significantly different from 0 for IC_{100} (0.68 [-0.38; 1.74]), indicating that the combined effect was just additive. Taken together, these results indicate that isolates enriched in the 4MBE variant have increased tolerance to RIF alone but also in combination with INH, possibly favoring treatment failure.

To explore a possible selective advantage of the 4MBE variant upon treatment, the dynamics of variant assemblies upon RIF exposure was monitored. The variant frequency thus increased

bioRxiv preprint doi: https://doi.org/10.1101/2020.05.22.110775; this version posted May 22, 2020. The copyright holder for this preprint (which was not certified by peer review) is the author/funder. All rights reserved. No reuse allowed without permission.

for II (from 1.5% to 30% ±13%) and for EI_{40} (from 39 ±5.0% to 55 ±6.7%) (Fig. 3D), consistent with the previous NGS experiments (Fig. 1A). Controlled bacterial assembly experiments, mixing IC_0 and IC_{100} at various ratios, yielded similar results (Fig. S1B). Interestingly, the variant frequency never reached 100%, as ddPCR allowed to detect at least 0.6% of the variant lacking C 3280555 G (IC_0) (Fig. S1B).

Efflux pumps are involved in RIF tolerance of the 4MBE variant

Given the involvement of efflux pumps in Mtb antibiotic tolerance [34, 35], the impact of efflux pump inhibitors (reserpine and valinomycin) on RIF tolerance of IC_0 and IC_{100} was explored. Whereas in the presence of valinomycin, there was a RIF dose-dependent increase in TTP for both IC_0 and IC_{100}, in the presence of reserpine a significant increase in TTP was found for IC_{100} only (ΔTTP 2.05 ± 0.29 days; Fig. 3E). These results suggest that efflux pumps are involved in RIF tolerance of the 4MBE variant, with a predominant role of reserpine-sensitive efflux pumps rather than valinomycin-sensitive ones. Consistently, quantitative RT-PCR experiments found higher *drrABC* and *p55* mRNA levels for IC_{100} compared to IC_0 (Fig. 3F). The DrrABC pump is known to display higher sensitivity to reserpine than valinomycin [36] and has been previously linked to RIF low-level resistance in Mtb without *rpoB* mutation [37].

4MBE variant frequency correlates with improved Mtb intra-macrophagic survival

As Mtb micro-diversity was also found to evolve upon macrophage infection (Fig. 1A), the abilities of intra-macrophage survival of II, EI_{40}, EI_{80}, and IC_{100} were explored at 6 h and 96 h post-infection (hpi).

The ability of IC_{100} to invade macrophages was significantly better ($32.10^4 \pm 11.10^4$ CFU/mL) than that of II ($6.10^4 \pm 2.10^4$ CFU/mL) at 6 hpi and this pattern was confirmed at 96 hpi, with 16 times more intracellular bacteria (Fig. 4A). Similarly, experiments conducted on the

bioRxiv preprint doi: https://doi.org/10.1101/2020.05.22.110775; this version posted May 22, 2020. The copyright holder for this preprint (which was not certified by peer review) is the author/funder. All rights reserved. No reuse allowed without permission.

controlled bacterial assembly found that the Mtb intracellular survival was directly related to the frequency of the 4MBE variant in the infecting inoculum (Fig. S1C). To further monitor Mtb variant composition upon host-pathogen interaction, the DNA of plated bacteria at 6 hpi and 96 hpi were recovered to assess the variant frequency by ddPCR (Figs. 4B and S1D). Upon infection by II and EI_{40}, there was an enrichment of the 4MBE variant, up to 36% and 64%, respectively, at 96 hpi, whereas variant frequency remained stable for EI_{80} (Fig. 4B). The same pattern was observed in controlled bacterial assembly (Fig. S1D). Interestingly, for infecting inocula containing 90% and 99% of the variant in the initial bacterial mix, the frequency remained stable and did not reach 100%, highlighting the role of Mtb diversity upon macrophage infection.

Improved intra-macrophagic survival of the 4MBE variant is due to phagolysosome avoidance and autophagic flux inhibition

Mtb intramacrophagic behavior of II, EI_{40}, EI_{80}, and IC_{100} was explored by confocal microscopy analysis at 24 hpi (Fig. 4). The improved Mtb intramacrophagic survival was confirmed by a significantly greater number of both infected cells and bacterial burden per cell, upon infection by EI_{40}, EI_{80}, and IC_{100} compared to II (Fig. S2).

To explore the mechanisms of Mtb intra-macrophage survival promoted by isolates enriched in 4MBE variant, phagolysosome activation and avoidance were first explored (Fig. 4C-E). Although no differences were observed in the number of cells with acidified compartments (Fig. 4C), upon infection by II, there were significantly more bacteria in acidified compartments (18.2% [7.1-38.3]) compared to the median values upon infection by EI_{40}, EI_{80}, and IC_{100} (Fig. 4D). Loading of infected macrophages with CCF4-AM, a fluorescence resonance energy transfer (FRET)-based assay, revealed that the blue/green signal was significantly lower upon infection by EI_{40}, EI_{80}, and IC_{100} compared to II (from 3.7 and 9.8 times less signal at 96 hpi;

bioRxiv preprint doi: https://doi.org/10.1101/2020.05.22.110775; this version posted May 22, 2020. The copyright holder for this preprint (which was not certified by peer review) is the author/funder. All rights reserved. No reuse allowed without permission.

Fig. 4E). This supports the notion that isolates enriched in the 4MBE variant avoid phagolysosomal fusion.

The autophagy activation and outcome were then explored. Chloroquine pretreatment showed an abolition of the differences of the proportion of cells with autophagy compartments between EI_{40}-, EI_{80}-, and IC_{100}-infected macrophages and II-infected macrophages. This suggests an inhibition of the autophagic flux for isolates enriched in the 4MBE variant (Fig. 4F). This was confirmed by the significant decrease in the proportion of acidified autophagy compartments upon infection by EI_{40}, EI_{80}, and IC_{100} compared to II (Fig. 4G). Furthermore, there was a decrease in autophagy magnitude upon infection by EI_{40}, EI_{80}, and IC_{100}, represented by a decrease of approximately 1.5 fold in LC3B puncta per cells for these strains compared to II (Fig. 4H). This indicate a weaker autophagy activation upon infection by isolates enriched in the 4MBE variant.

Taken together, these results support that the better intracellular survival of isolates enriched in the 4MBE variant during macrophage infection is driven by the increase of phagolysosome avoidance and the decrease of both autophagic flux and autophagy activation.

Macrophage apoptosis and inflammatory response are exacerbated upon infection by isolates containing high relative frequency of the 4MBE variant

Macrophage transcriptome analysis showed that 677 genes were differentially expressed between macrophages infected by II and those infected by either EI_{40} or EI_{80}. Three distinct population clusters, II, EI_{40}, and EI_{80}, were recognized by principal component analysis (PCA; Fig. S3). The first principal component (46.4% of the variance) allowed a discrimination of II-infected macrophages from EI-infected macrophages, while the second one (17.7% of the variance) allowed discrimination of EI_{40}- and EI_{80}-infected macrophages.

bioRxiv preprint doi: https://doi.org/10.1101/2020.05.22.110775; this version posted May 22, 2020. The copyright holder for this preprint (which was not certified by peer review) is the author/funder. All rights reserved. No reuse allowed without permission.

A total of 337 differentially expressed genes between macrophages infected by II and EI_{40} or EI_{80} were selected to build a heatmap, showing clustering according to biological replicates and to the frequency of the 4MBE variant in the Mtb infecting inoculum (Fig. 5A). The differentially expressed genes were classified into nine functional categories involved in Mtb macrophage response. Consistent with the macrophage infection experiments, actin cytoskeleton, autophagy, and phagolysosome pathways were found to be dysregulated upon infection by EI_{40} and EI_{80} compared to II. Moreover, there was also a dysregulation of inflammatory response, apoptosis and cell cycle, mitochondrial metabolism, lipid metabolism, and T cell signaling pathways.

In order to explore cell death mechanisms, necrosis (Fig. 5B) and apoptosis (Fig. 5C) of macrophages were assessed upon infection by II, EI_{40}, and EI_{80}, and IC_{100} at 24 and 96 hpi. At 96 hpi, there was no significant difference between II- (48% ± 3.0%) and EI_{40}-induced necrosis rates (51.6% ± 3.1%). By contrast, the necrotic effect upon EI_{80} (55.2% ± 6.2%) and IC_{100} (64.9% ± 3.5%) infections was significantly greater than that obtained upon II infections (Fig. 5B). Furthermore, apoptosis was also significantly higher upon infection by EI_{80} and IC_{100} compared to II (Fig. 5C). Thus, macrophage cell death level increased with the frequency of the 4MBE variant in the Mtb infecting inoculum.

Cytokines (TNF-α, IL-6, IL-1β, IFN-γ) and chemokines (RANTES (CCL5) and interferon gamma-induced protein 10 (IP-10)) production were then measured at 6 hpi (Fig. S4), 24 hpi (Fig. 5D-I), and 96 hpi (Fig. S5) to explore macrophage inflammatory response. At 24hpi, there was a significant increase in the inflammatory response of macrophages upon infection by EI_{40}, EI_{80}, and IC_{100} compared to II, and this effect was constantly more pronounced for IC_{100} (Fig. 5D-I). Upon infection by IC_{100} there was a significant increase in TNF-α production by macrophages from 6 to 96 hpi (Fig. 5D, S4A, and S5A) and overall a sustained inflammatory response at 96 hpi (Fig. S5). Finally, chemokine signals were significantly increased upon

bioRxiv preprint doi: https://doi.org/10.1101/2020.05.22.110775; this version posted May 22, 2020. The copyright holder for this preprint (which was not certified by peer review) is the author/funder. All rights reserved. No reuse allowed without permission.

infection by IC_{100} (Fig. 7H-I). Overall, the macrophage pro-inflammatory response was stronger (in terms of intensity and duration) upon infection by EI_{40}, EI_{80}, and IC_{100} than by II, the higher the frequency of the 4MBE variant in the infecting inoculum, the higher the inflammatory response.

DISCUSSION

The objective of the present study was to address the role of Mtb micro-diversity and its possible link with anti-TB treatment response. We therefore monitored Mtb micro-diversity during the course of the adaptive response of clinical isolates to environment variations consistent with TB infection and treatment. We explored 16 clinical pan-susceptible isolates responsible for pulmonary TB with persistent positive culture upon treatment and our results showed that micro-diversity in Mtb is not restricted to the few previously reported cases [5, 10, 11, 13, 38, 39]. Interestingly, WGS of isolated colonies allowed detection of additional SNPs when compared to WGS performed on the whole bacterial population, suggesting that more knowledge concerning Mtb diversity will be enabled in the future through the use of deeper sequencing.

We then focused on a single clinical isolate and highlighted the plasticity of its genetic micro-diversity, which presented a changing pattern of variant assembly depending on the experimental setting (intra-macrophage infection, antibiotic stress). Interestingly, a variant (called hereafter 4MBE variant) which was present at low frequency in the initial Mtb clinical isolate, became predominant under the stress conditions tested. Using a set of complementary approaches we were able to show that this type of variant displayed tolerance to anti-TB treatment.

It was recently suggested that numerous variants emerge and then disappear during the course of infection and treatment within individual patients [38, 39]. The minor variant identified in

bioRxiv preprint doi: https://doi.org/10.1101/2020.05.22.110775; this version posted May 22, 2020. The copyright holder for this preprint (which was not certified by peer review) is the author/funder. All rights reserved. No reuse allowed without permission.

the present study may be beneficial during some stages of the Mtb infection lifecycle and, in parallel, may be deleterious in other conditions, explaining its potentially transient emergence. We found that this variant features a particular lipid profile consisting of enriched tetramethyl-branched mycocerosates, a PDIM component. Being located at the interface between the bacterium and the host, PDIM play important roles in directing host-pathogen interactions and are involved at many pathophysiological steps [25, 40–42]. Nevertheless, studies showed that PDIM and mycolic acids were down-regulated during extended intracellular infection to the benefit of other multimethyl-branched fatty acids [43–45]. In addition, the results presented herein clearly demonstrated more intense macrophage inflammatory response during infection with isolates containing a high frequency of the 4MBE variant, which could be deleterious during human lung infection. Consistently, a significant increase in macrophage cell death was also found, particularly concerning apoptosis occurrence, upon infection by these isolates. Apoptosis is generally regarded as a protective response, whereas necrosis is thought to favor inflammation and disease progression [46–48]. In that respect, macrophage apoptosis could be considered a limitative mechanism, preventing the spread of this variant. Taken together, the results of the present study suggest that isolates containing the 4MBE variant could mainly favor infection initiation while other variants that have yet to be identified may be more involved in long-term infection.

The main feature of the variant detected and studied herein, which could be discriminated from the major one based on WGS data, was a non-synonymous polymorphism of *mas*, a gene belonging to the PDIM cluster, and was thus not related to a canonical drug-resistant locus. Although the search of public databases did not allow to identify this fixed polymorphism in other Mtb genomes, we were able to detect it, at a frequency (~1%) undetectable by WGS, in another Mtb clinical isolate by performing ddPCR assay. Among the 140 clinical isolates tested by ddPCR screening, this particular isolate was multi-drug resistant (MDR) belonging to the

bioRxiv preprint doi: https://doi.org/10.1101/2020.05.22.110775; this version posted May 22, 2020. The copyright holder for this preprint (which was not certified by peer review) is the author/funder. All rights reserved. No reuse allowed without permission.

Euro-American lineage (data not shown). It is thus possible that this type of variant may play a role along the successive steps leading to MDR-TB, as it also showed increased RIF tolerance. The antibacterial effect of RIF alone and in combination with INH was different on the isolates enriched in 4MBE variant, with a decreased efficacy of RIF alone and loss of synergistic activity when in combination with INH. This suggests that optimal management may require higher drug doses in cases of persistent infection with Mtb isolates containing such variants.

When focusing on resistance emergence, current diagnostic tools are based on the detection of fixed or unfixed variants in loci involved in drug resistance, to adapt treatment as early as possible [49, 50]. Likewise, our results suggest that the emergence of unfixed variants in loci not necessarily linked to canonical drug-resistance could also help as diagnostic markers. Indeed, features associated with Mtb tolerance, possibly through mutations affecting efflux pump expression, have been suggested to be potential pre-resistant markers [51–53]. Interestingly, the tolerance exhibited by the isolates enriched in 4MBE variant was probably supported by the differential expression of efflux pumps which have been shown to be involved in both PDIM and RIF transport [35, 54]. Herein we show for the first time that such a minor variant may be associated with drug-tolerance, promote treatment failure as predicted by pharmacological modelling, and eventually lead to drug-resistance. Interestingly, even under extreme experimental conditions, the diversity in variants was always maintained, suggesting the possibility of a strong functional complementarity between variants of the Mtb bacterial population during disease dynamics. This emphasizes the importance of Mtb micro-diversity, which could become a useful diagnostic tool to predict which patients are at risk of poor response to anti-TB treatment. These patients may require personalized dosing and therapeutic management in order to improve the outcome and to effectively prevent MDR-TB emergence.

In-depth analysis of clinical isolates coupled to the development of *in vitro* models to assess minor variants with increased fitness, antibiotic tolerance, or enhanced virulence, could help

bioRxiv preprint doi: https://doi.org/10.1101/2020.05.22.110775; this version posted May 22, 2020. The copyright holder for this preprint (which was not certified by peer review) is the author/funder. All rights reserved. No reuse allowed without permission.

identify mutations responsible for treatment failure, better understand Mtb pathogenicity, and ultimately, through the use of fine-tuned diagnosis tools, allow personalized TB management.

ACKNOWLEDGMENTS

This work was supported by the LABEX ECOFECT (ANR-11-LABX-0048) of Université de Lyon, within the program "Investissements d'Avenir" (ANR-11-IDEX-0007) operated by the French national research agency (Agence nationale de la recherché, ANR).

The authors thank Philip Robinson and Véréna Landel (DRCI, Hospices Civils de Lyon) for help in manuscript preparation.

Author Contributions

Conceptualization: C.Ge., S.G., O.D.; Methodology: C.Ge., C.Gi., S.G., O.D.; Software: C.Ge., J-L.B., J-B.C., E.W.; Investigation and validation: C.Ge., E.H., A.B., J.H., V.B., F.B., M.G.; Data analysis: C.Ge., A.B., E.H., F.B., M.G., C.Gi., S.G., O.D.; Data interpretation: C.Ge., A.B., E.H., J-L.B., J.H., S.V., C.Gi., S.G., O.D.; Visualization: C.Ge, E.H., S.G., O.D.; Writing – Original Draft: C.Ge., S.G., O.D.; Writing – Review & Editing: All authors; Funding Acquisition: C.Ge., J-L. B., S.V., G.L., S.G., O.D.

Compliance with ethical standards

Conflict of Interests

The authors declare that they have no conflict of interest.

REFERENCES:

1. World Health Organization, Geneva | Global tuberculosis report 2019. *WHO*. http://www.who.int/tb/publications/global_report/en/. Accessed 28 Oct 2019.

bioRxiv preprint doi: https://doi.org/10.1101/2020.05.22.110775; this version posted May 22, 2020. The copyright holder for this preprint (which was not certified by peer review) is the author/funder. All rights reserved. No reuse allowed without permission.

2. Wallis RS, Patil S, Cheon S-H, Edmonds K, Phillips M, Perkins MD, et al. Drug Tolerance in Mycobacterium tuberculosis. *Antimicrob Agents Chemother* 1999; **43**: 2600–2606.

3. Levin-Reisman I, Ronin I, Gefen O, Braniss I, Shoresh N, Balaban NQ. Antibiotic tolerance facilitates the evolution of resistance. *Science* 2017; **355**: 826–830.

4. Brown AC, Bryant JM, Einer-Jensen K, Holdstock J, Houniet DT, Chan JZM, et al. Rapid Whole-Genome Sequencing of Mycobacterium tuberculosis Isolates Directly from Clinical Samples. *Journal of Clinical Microbiology* 2015; **53**: 2230–2237.

5. Casali N, Broda A, Harris SR, Parkhill J, Brown T, Drobniewski F. Whole Genome Sequence Analysis of a Large Isoniazid-Resistant Tuberculosis Outbreak in London: A Retrospective Observational Study. *PLoS Med* 2016; **13**.

6. Doyle RM, Burgess C, Williams R, Gorton R, Booth H, Brown J, et al. Direct Whole-Genome Sequencing of Sputum Accurately Identifies Drug-Resistant *Mycobacterium tuberculosis* Faster than MGIT Culture Sequencing. *Journal of Clinical Microbiology* 2018; **56**.

7. Genestet C, Hodille E, Westeel E, Ginevra C, Ader F, Venner S, et al. Subcultured Mycobacterium tuberculosis isolates on different growth media are fully representative of bacteria within clinical samples. *Tuberculosis (Edinb)* 2019; **116**: 61–66.

8. Shockey AC, Dabney J, Pepperell CS. Effects of Host, Sample, and in vitro Culture on Genomic Diversity of Pathogenic Mycobacteria. *Front Genet* 2019; **10**.

9. Votintseva AA, Bradley P, Pankhurst L, del Ojo Elias C, Loose M, Nilgiriwala K, et al. Same-Day Diagnostic and Surveillance Data for Tuberculosis via Whole-Genome Sequencing of Direct Respiratory Samples. *Journal of Clinical Microbiology* 2017; **55**: 1285–1298.

bioRxiv preprint doi: https://doi.org/10.1101/2020.05.22.110775; this version posted May 22, 2020. The copyright holder for this preprint (which was not certified by peer review) is the author/funder. All rights reserved. No reuse allowed without permission.

10. Lieberman TD, Wilson D, Misra R, Xiong LL, Moodley P, Cohen T, et al. Genomic diversity in autopsy samples reveals within-host dissemination of HIV-associated *Mycobacterium tuberculosis*. *Nature Medicine* 2016; **22**: 1470–1474.

11. O'Neill MB, Mortimer TD, Pepperell CS. Diversity of Mycobacterium tuberculosis across Evolutionary Scales. *PLOS Pathogens* 2015; **11**: e1005257.

12. Pérez-Lago L, Comas I, Navarro Y, González-Candelas F, Herranz M, Bouza E, et al. Whole genome sequencing analysis of intrapatient microevolution in Mycobacterium tuberculosis: potential impact on the inference of tuberculosis transmission. *J Infect Dis* 2014; **209**: 98–108.

13. Vargas R, Freschi L, Marin M, Epperson LE, Smith M, Oussenko I, et al. In-host population dynamics of M. tuberculosis during treatment failure. *bioRxiv* 2019; 726430.

14. Copin R, Wang X, Louie E, Escuyer V, Coscolla M, Gagneux S, et al. Within Host Evolution Selects for a Dominant Genotype of Mycobacterium tuberculosis while T Cells Increase Pathogen Genetic Diversity. *PLOS Pathogens* 2016; **12**: e1006111.

15. Navarro Y, Pérez-Lago L, Sislema F, Herranz M, de Juan L, Bouza E, et al. Unmasking subtle differences in the infectivity of microevolved Mycobacterium tuberculosis variants coinfecting the same patient. *Int J Med Microbiol* 2013; **303**: 693–696.

16. Ailloud F, Didelot X, Woltemate S, Pfaffinger G, Overmann J, Bader RC, et al. Within-host evolution of Helicobacter pylori shaped by niche-specific adaptation, intragastric migrations and selective sweeps. *Nat Commun* 2019; **10**: 1–13.

17. Azarian T, Ridgway JP, Yin Z, David MZ. Long-Term Intrahost Evolution of Methicillin Resistant Staphylococcus aureus Among Cystic Fibrosis Patients With Respiratory Carriage. *Front Genet* 2019; **10**.

bioRxiv preprint doi: https://doi.org/10.1101/2020.05.22.110775; this version posted May 22, 2020. The copyright holder for this preprint (which was not certified by peer review) is the author/funder. All rights reserved. No reuse allowed without permission.

18. Winstanley C, O'Brien S, Brockhurst MA. Pseudomonas aeruginosa Evolutionary Adaptation and Diversification in Cystic Fibrosis Chronic Lung Infections. *Trends Microbiol* 2016; **24**: 327–337.

19. Bowness R, Boeree MJ, Aarnoutse R, Dawson R, Diacon A, Mangu C, et al. The relationship between Mycobacterium tuberculosis MGIT time to positivity and cfu in sputum samples demonstrates changing bacterial phenotypes potentially reflecting the impact of chemotherapy on critical sub-populations. *J Antimicrob Chemother* 2015; **70**: 448–455.

20. Genestet C, Ader F, Pichat C, Lina G, Dumitrescu O, Goutelle S, et al. Combined Antibacterial Effect of Isoniazid and Rifampicin on Four Mycobacterium tuberculosis Strains: in Vitro Experiments and Response-Surface Modeling. *Antimicrob Agents Chemother* 2017.

21. Genestet C, Tatai C, Berland J-L, Claude J-B, Westeel E, Hodille E, et al. Prospective Whole-Genome Sequencing in Tuberculosis Outbreak Investigation, France, 2017–2018. *Emerging Infectious Diseases* 2019; **25**: 589–592.

22. Nicoara SC, Minnikin DE, Lee OCY, O'Sullivan DM, McNerney R, Pillinger CT, et al. Development and optimization of a gas chromatography/mass spectrometry method for the analysis of thermochemolytic degradation products of phthiocerol dimycocerosate waxes found in Mycobacterium tuberculosis. *Rapid Commun Mass Spectrom* 2013; **27**: 2374–2382.

23. O'Sullivan DM, Nicoara SC, Mutetwa R, Mungofa S, Lee OY-C, Minnikin DE, et al. Detection of Mycobacterium tuberculosis in Sputum by Gas Chromatography-Mass Spectrometry of Methyl Mycocerosates Released by Thermochemolysis. *PLOS ONE* 2012; **7**: e32836.

bioRxiv preprint doi: https://doi.org/10.1101/2020.05.22.110775; this version posted May 22, 2020. The copyright holder for this preprint (which was not certified by peer review) is the author/funder. All rights reserved. No reuse allowed without permission.

24. Genestet C, Bernard-Barret F, Hodille E, Ginevra C, Ader F, Goutelle S, et al. Antituberculous drugs modulate bacterial phagolysosome avoidance and autophagy in Mycobacterium tuberculosis-infected macrophages. *Tuberculosis (Edinb)* 2018; **111**: 67–70.

25. Quigley J, Hughitt VK, Velikovsky CA, Mariuzza RA, El-Sayed NM, Briken V. The Cell Wall Lipid PDIM Contributes to Phagosomal Escape and Host Cell Exit of Mycobacterium tuberculosis. *mBio* 2017; **8**: e00148-17.

26. Simeone R, Bobard A, Lippmann J, Bitter W, Majlessi L, Brosch R, et al. Phagosomal Rupture by Mycobacterium tuberculosis Results in Toxicity and Host Cell Death. *PLOS Pathogens* 2012; **8**: e1002507.

27. Koo M-S, Subbian S, Kaplan G. Strain specific transcriptional response in Mycobacterium tuberculosis infected macrophages. *Cell Commun Signal* 2012; **10**: 2.

28. Trapnell C, Williams BA, Pertea G, Mortazavi A, Kwan G, van Baren MJ, et al. Transcript assembly and abundance estimation from RNA-Seq reveals thousands of new transcripts and switching among isoforms. *Nat Biotechnol* 2010; **28**: 511–515.

29. Dray S, Dufour A-B. The ade4 Package: Implementing the Duality Diagram for Ecologists. *Journal of Statistical Software* 2007; **22**: 1–20.

30. Babicki S, Arndt D, Marcu A, Liang Y, Grant JR, Maciejewski A, et al. Heatmapper: web-enabled heat mapping for all. *Nucleic Acids Res* 2016; **44**: W147–W153.

31. Herbst DA, Jakob RP, Zähringer F, Maier T. Mycocerosic acid synthase exemplifies the architecture of reducing polyketide synthases. *Nature* 2016; **531**: 533–537.

32. Trivedi OA, Arora P, Vats A, Ansari MZ, Tickoo R, Sridharan V, et al. Dissecting the mechanism and assembly of a complex virulence mycobacterial lipid. *Mol Cell* 2005; **17**: 631–643.

bioRxiv preprint doi: https://doi.org/10.1101/2020.05.22.110775; this version posted May 22, 2020. The copyright holder for this preprint (which was not certified by peer review) is the author/funder. All rights reserved. No reuse allowed without permission.

33. Redman JE, Shaw MJ, Mallet AI, Santos AL, Roberts CA, Gernaey AM, et al. Mycocerosic acid biomarkers for the diagnosis of tuberculosis in the Coimbra Skeletal Collection. *Tuberculosis (Edinb)* 2009; **89**: 267–277.

34. Machado D, Coelho TS, Perdigão J, Pereira C, Couto I, Portugal I, et al. Interplay between Mutations and Efflux in Drug Resistant Clinical Isolates of Mycobacterium tuberculosis. *Front Microbiol* 2017; **8**.

35. Te Brake LHM, de Knegt GJ, de Steenwinkel JE, van Dam TJP, Burger DM, Russel FGM, et al. The Role of Efflux Pumps in Tuberculosis Treatment and Their Promise as a Target in Drug Development: Unraveling the Black Box. *Annu Rev Pharmacol Toxicol* 2018; **58**: 271–291.

36. Sarathy JP, Dartois V, Lee EJD. The Role of Transport Mechanisms in Mycobacterium Tuberculosis Drug Resistance and Tolerance. *Pharmaceuticals* 2012; **5**: 1210–1235.

37. Pang Y, Lu J, Wang Y, Song Y, Wang S, Zhao Y. Study of the Rifampin Monoresistance Mechanism in Mycobacterium tuberculosis. *Antimicrobial Agents and Chemotherapy* 2013; **57**: 893–900.

38. Black PA, de Vos M, Louw GE, van der Merwe RG, Dippenaar A, Streicher EM, et al. Whole genome sequencing reveals genomic heterogeneity and antibiotic purification in Mycobacterium tuberculosis isolates. *BMC Genomics* 2015; **16**: 857.

39. Trauner A, Liu Q, Via LE, Liu X, Ruan X, Liang L, et al. The within-host population dynamics of Mycobacterium tuberculosis vary with treatment efficacy. *Genome Biology* 2017; **18**: 71.

40. Augenstreich J, Arbues A, Simeone R, Haanappel E, Wegener A, Sayes F, et al. ESX-1 and phthiocerol dimycocerosates of Mycobacterium tuberculosis act in concert to cause phagosomal rupture and host cell apoptosis. *Cellular Microbiology* 2017; **19**: e12726.

bioRxiv preprint doi: https://doi.org/10.1101/2020.05.22.110775; this version posted May 22, 2020. The copyright holder for this preprint (which was not certified by peer review) is the author/funder. All rights reserved. No reuse allowed without permission.

41. Jackson M. The Mycobacterial Cell Envelope—Lipids. *Cold Spring Harb Perspect Med* 2014; **4**.

42. Queval CJ, Brosch R, Simeone R. The Macrophage: A Disputed Fortress in the Battle against Mycobacterium tuberculosis. *Front Microbiol* 2017; **8**.

43. Rohde KH, Abramovitch RB, Russell DG. Mycobacterium tuberculosis Invasion of Macrophages: Linking Bacterial Gene Expression to Environmental Cues. *Cell Host & Microbe* 2007; **2**: 352–364.

44. Rohde KH, Veiga DFT, Caldwell S, Balázsi G, Russell DG. Linking the Transcriptional Profiles and the Physiological States of Mycobacterium tuberculosis during an Extended Intracellular Infection. *PLOS Pathogens* 2012; **8**: e1002769.

45. Singh A, Crossman DK, Mai D, Guidry L, Voskuil MI, Renfrow MB, et al. Mycobacterium tuberculosis WhiB3 Maintains Redox Homeostasis by Regulating Virulence Lipid Anabolism to Modulate Macrophage Response. *PLoS Pathog* 2009; **5**.

46. Parandhaman DK, Narayanan S. Cell death paradigms in the pathogenesis of Mycobacterium tuberculosis infection. *Front Cell Infect Microbiol* 2014; **4**.

47. Teng O, Ang CKE, Guan XL. Macrophage–Bacteria Interactions—A Lipid-Centric Relationship. *Front Immunol* 2017; **8**.

48. Zhai W, Wu F, Zhang Y, Fu Y, Liu Z. The Immune Escape Mechanisms of Mycobacterium Tuberculosis. *Int J Mol Sci* 2019; **20**.

49. Ng KCS, Supply P, Cobelens FGJ, Gaudin C, Gonzalez-Martin J, Jong BC de, et al. How Well Do Routine Molecular Diagnostics Detect Rifampin Heteroresistance in Mycobacterium tuberculosis? *Journal of Clinical Microbiology* 2019; **57**: e00717-19.

50. Sun G, Luo T, Yang C, Dong X, Li J, Zhu Y, et al. Dynamic population changes in Mycobacterium tuberculosis during acquisition and fixation of drug resistance in patients. *J Infect Dis* 2012; **206**: 1724–1733.

bioRxiv preprint doi: https://doi.org/10.1101/2020.05.22.110775; this version posted May 22, 2020. The copyright holder for this preprint (which was not certified by peer review) is the author/funder. All rights reserved. No reuse allowed without permission.

51. Coll F, Phelan J, Hill-Cawthorne GA, Nair MB, Mallard K, Ali S, et al. Genome-wide analysis of multi- and extensively drug-resistant Mycobacterium tuberculosis. *Nat Genet* 2018; **50**: 307–316.

52. Pasipanodya JG, Gumbo T. A new evolutionary and pharmacokinetic–pharmacodynamic scenario for rapid emergence of resistance to single and multiple anti-tuberculosis drugs. *Current Opinion in Pharmacology* 2011; **11**: 457–463.

53. Schmalstieg AM, Srivastava S, Belkaya S, Deshpande D, Meek C, Leff R, et al. The Antibiotic Resistance Arrow of Time: Efflux Pump Induction Is a General First Step in the Evolution of Mycobacterial Drug Resistance. *Antimicrobial Agents and Chemotherapy* 2012; **56**: 4806–4815.

54. Domenech P, Reed MB. Rapid and spontaneous loss of phthiocerol dimycocerosate (PDIM) from Mycobacterium tuberculosis grown in vitro: implications for virulence studies. *Microbiology* 2009; **155**: 3532–3543.

bioRxiv preprint doi: https://doi.org/10.1101/2020.05.22.110775; this version posted May 22, 2020. The copyright holder for this preprint (which was not certified by peer review) is the author/funder. All rights reserved. No reuse allowed without permission.

660 **FIGURE LEGENDS**

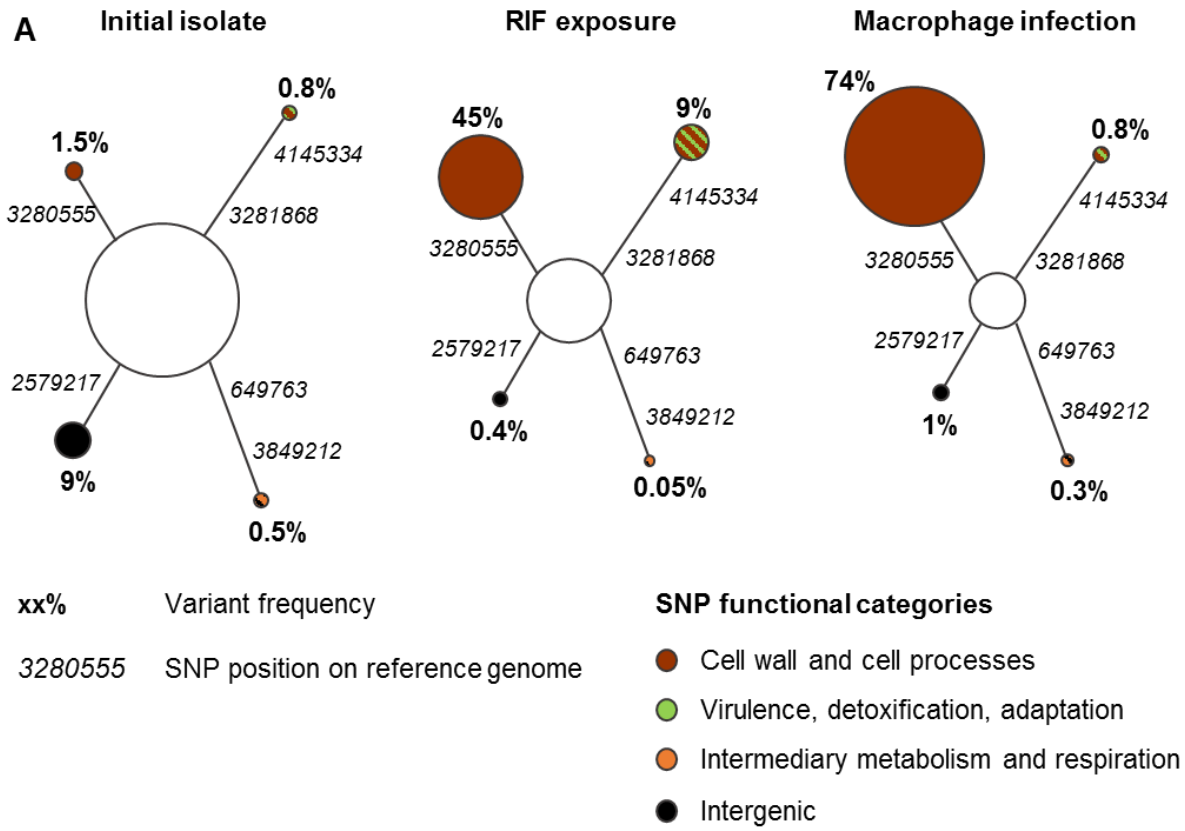

B

Name	Origin	Stress applied to initial isolate	Mean frequency of C 3280555 G variant (%)
II	Clinical isolate	None	1.5
EI_{40}	Clinical isolate	RIF exposure	40
EI_{80}	Clinical isolate	Macrophage infection	80
IC_0	Clone of II	N/A	0
IC_{100}	Clone of II	N/A	100

II: initial isolate; EI: evolved isolate; IC: initial clone; $_{xx}$: frequency of C 3280555 G variant; N/A: Not Applicable

661

662 **Fig. 1: A minor variant of Mtb clinical isolate is selected in response to both rifampicin**

663 **exposure and macrophage infection.**

664 (**a**) Minimum spanning trees (MST) of the initial clinical isolate, "initial isolate", after 4 weeks

665 of RIF exposure at 1xMIC or after 7 days of macrophage infection at a multiplicity of infection

bioRxiv preprint doi: https://doi.org/10.1101/2020.05.22.110775; this version posted May 22, 2020. The copyright holder for this preprint (which was not certified by peer review) is the author/funder. All rights reserved. No reuse allowed without permission.

(MOI) of 10:1 (bacteria:cells) assessed by targeted NGS with coverage ranging from 10 000 to 36 000x. (**b**) Characteristics of the 5 strains used in this study.

bioRxiv preprint doi: https://doi.org/10.1101/2020.05.22.110775; this version posted May 22, 2020. The copyright holder for this preprint (which was not certified by peer review) is the author/funder. All rights reserved. No reuse allowed without permission.

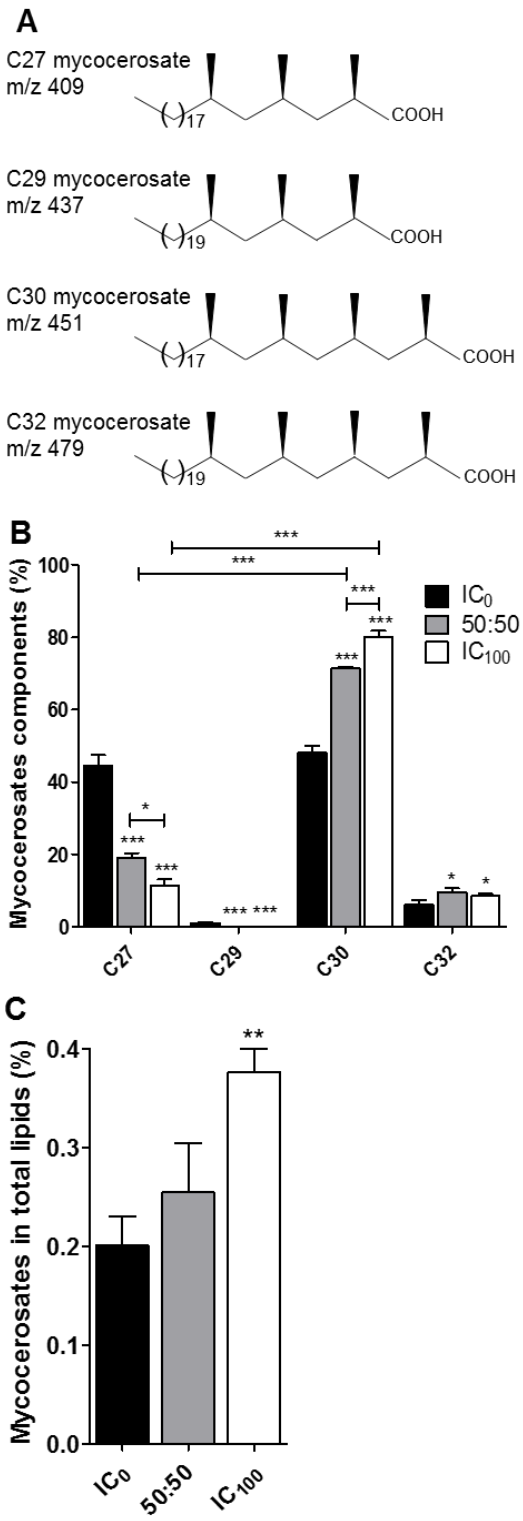

Fig. 2: The 4MBE variant overexpresses mycocerosates and more particularly the tetramethyl-branched components of mycocerosates.

(**a**) Molecular structures of C27, C29, C30 and C32 mycocerosate components from Mtb. (**b-c**) The lipid profile of IC_0 and IC_{100} and a half-half mixture (50:50) of these clones were compared.

bioRxiv preprint doi: https://doi.org/10.1101/2020.05.22.110775; this version posted May 22, 2020. The copyright holder for this preprint (which was not certified by peer review) is the author/funder. All rights reserved. No reuse allowed without permission.

(**b**) Proportion of mycocerosate components regarding total mycocerosates were explored by gas chromatography-mass spectrometry (GC-MS) and obtained from ion chromatograms showing the fragment ions at m/z 409, 437, 451 and 479 representing mycocerosate components C27, C29, C30 and C32, respectively. (**c**) Proportion of mycocerosates in total lipids were obtained from ion chromatograms showing all fatty acids detected by GC-MS. Values for each condition are the mean ± SD of at least three independent experiments. Means were compared using One-Way ANOVA followed by Bonferroni's test.

bioRxiv preprint doi: https://doi.org/10.1101/2020.05.22.110775; this version posted May 22, 2020. The copyright holder for this preprint (which was not certified by peer review) is the author/funder. All rights reserved. No reuse allowed without permission.

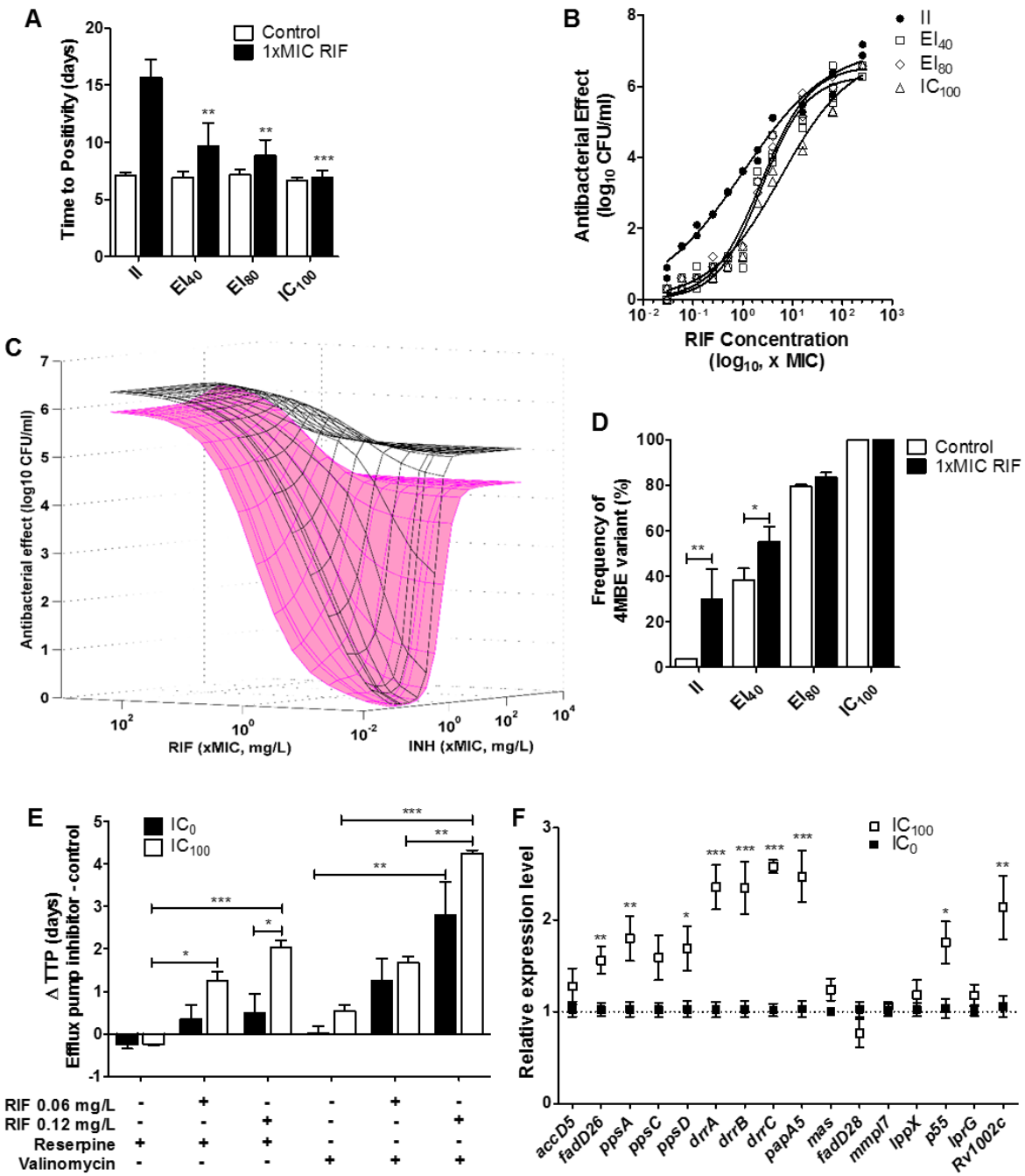

Fig. 3: The 4MBE variant is tolerant to RIF alone and in combination with INH.

(**a**) Mycobacterial growth in absence (Ctrl) or presence of RIF (1xMIC RIF) is expressed in time to positivity (TTP) in BACTEC system. All conditions were compared to II. (**b**) Time-kill data were determined after 7 days of RIF exposure at various concentrations. Fit of the Hill pharmacodynamic model to RIF time-kill data, the solid lines are the best fit lines. The y-axis represents the difference in $\log_{10}$ CFU/mL relative to control (C = 0) from a duplicate

bioRxiv preprint doi: https://doi.org/10.1101/2020.05.22.110775; this version posted May 22, 2020. The copyright holder for this preprint (which was not certified by peer review) is the author/funder. All rights reserved. No reuse allowed without permission.

experiment. (**c**) Superposition of response surface models of the combined antibacterial effect of INH and RIF against IC_0 (black) and IC_{100} (pink). A total of 142 measures of the effect of RIF and INH alone or in combination were performed, and results were analyzed using the Minto response surface model. The surfaces represent the model-based predicted effect, representing the antibacterial effect measured after 7 days of exposure. (**d**) After 4 weeks of incubation without (Ctrl) or with RIF (1xMIC RIF), the change in the 4MBE variant frequency on plated bacteria was assessed by ddPCR as described in Methods section. (**e**) IC_0 and IC_{100} were incubated with either reserpine (100 µM) or valinomycin (0.1 µM) in the absence or presence of RIF at 0.06 mg/L or 0.12 mg/L, or without efflux pump inhibitor as control. Results are expressed in delta of TTP between cultures in presence and absence of efflux pump inhibitor. (**f**) Quantitative RT-PCR were performed and normalized to 16S rRNA from the same sample. These results represent the differences in the mRNA levels detected in IC_{100} relative to the mRNA level of IC_0 upon RIF exposure at 1/8xMIC. (**a** and **d** – **f**) Values for each condition are the mean ± SD of at least three independent experiments. Means were compared using one-way ANOVA followed by Bonferroni's test or using the Student's t-test, when appropriate.

bioRxiv preprint doi: https://doi.org/10.1101/2020.05.22.110775; this version posted May 22, 2020. The copyright holder for this preprint (which was not certified by peer review) is the author/funder. All rights reserved. No reuse allowed without permission.

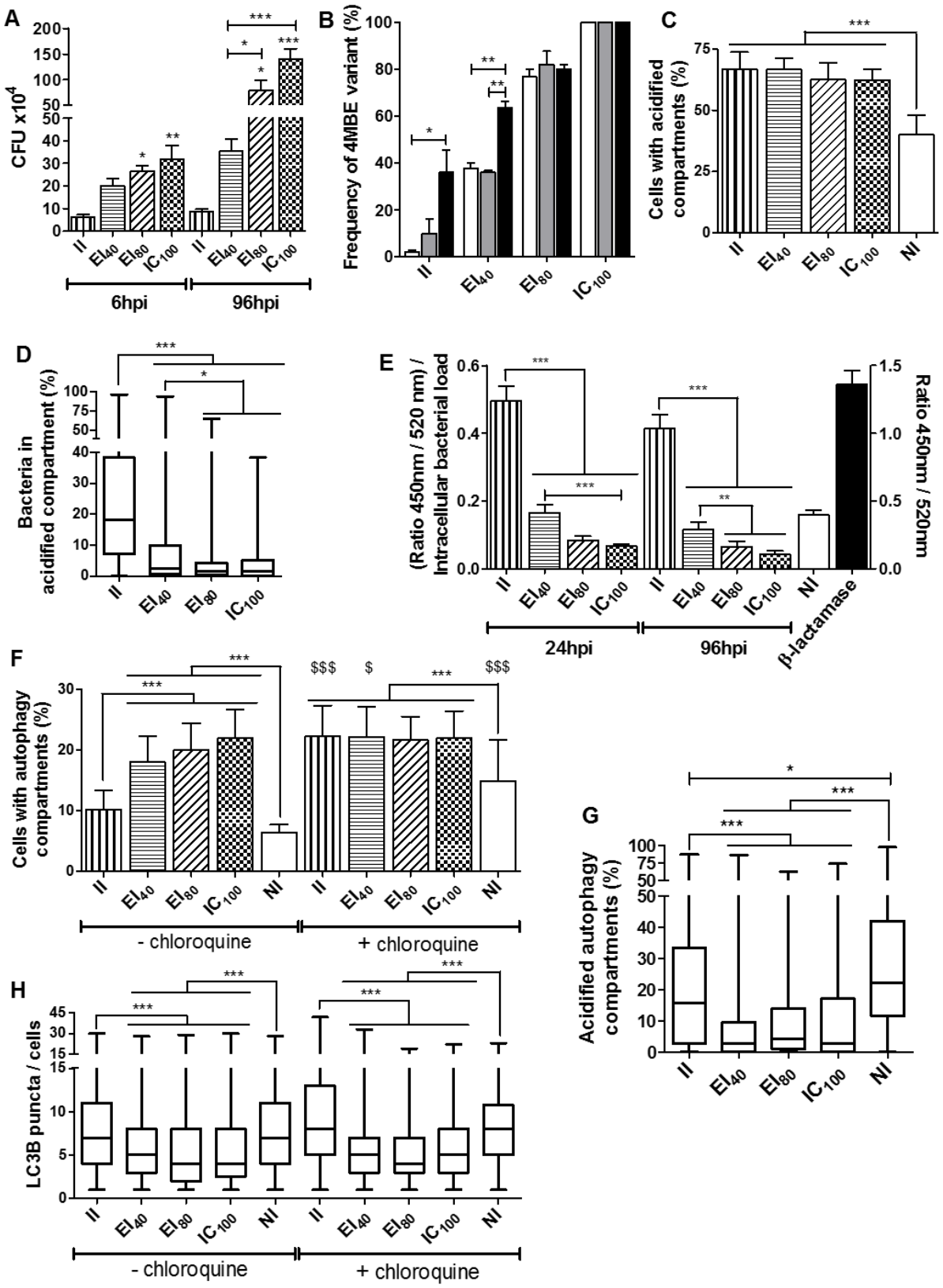

Fig. 4: Improved intra-macrophagic survival of the 4MBE variant is due to phagolysosome avoidance and autophagic flux inhibition.

bioRxiv preprint doi: https://doi.org/10.1101/2020.05.22.110775; this version posted May 22, 2020. The copyright holder for this preprint (which was not certified by peer review) is the author/funder. All rights reserved. No reuse allowed without permission.

Macrophages were infected by II, EI_{40}, EI_{80} and IC_{100} at a MOI of 10:1. (**a**) At 6 and 96 hpi, macrophages were lysed for intracellular CFU counting (*significantly different from the control (II)) and (**b**) the change in the 4MBE variant frequency on plated bacteria was assessed by ddPCR as described in the Methods section. Values for each condition are the mean ± SD of three independent experiments. Means were compared using One-Way ANOVA followed by Bonferroni test. (**c-d** and **f-h**) At 24 hpi, cells were stained with LysoTracker Red DND-99, anti-Mtb coupled FITC and anti-LC3B coupled Dy-Light 650 antibodies. (**c** and **f**) Cells with acidified (**c**) or autophagy compartments (**f**) were determined across at least 10 confocal images, containing between 30 and 80 cells per image, per replicate. (**d, g, h**) Percentage of bacteria in acidified compartments (**d**), LC3B puncta per cells (**g**) and percentage of acidified autophagy compartments (**h**) were determined across at least 40 cells per replicate. (**f** and **h**) Three hours before staining, cells were incubated with chloroquine, then macrophages were stained and analyzed as previously described. (**e**) Infected macrophages were loaded with CCF4-AM at 24 and 96 hpi to analyze 450nm/520nm ratio normalized on bacterial load. Values for each condition are the median ± interquartile range (IQR) of at least three independent experiments. Statistical significance was determined using Kruskal-Wallis analysis, using Dunn's Multiple Comparison Test. $ Significantly different from condition without chloroquine.

bioRxiv preprint doi: https://doi.org/10.1101/2020.05.22.110775; this version posted May 22, 2020. The copyright holder for this preprint (which was not certified by peer review) is the author/funder. All rights reserved. No reuse allowed without permission.

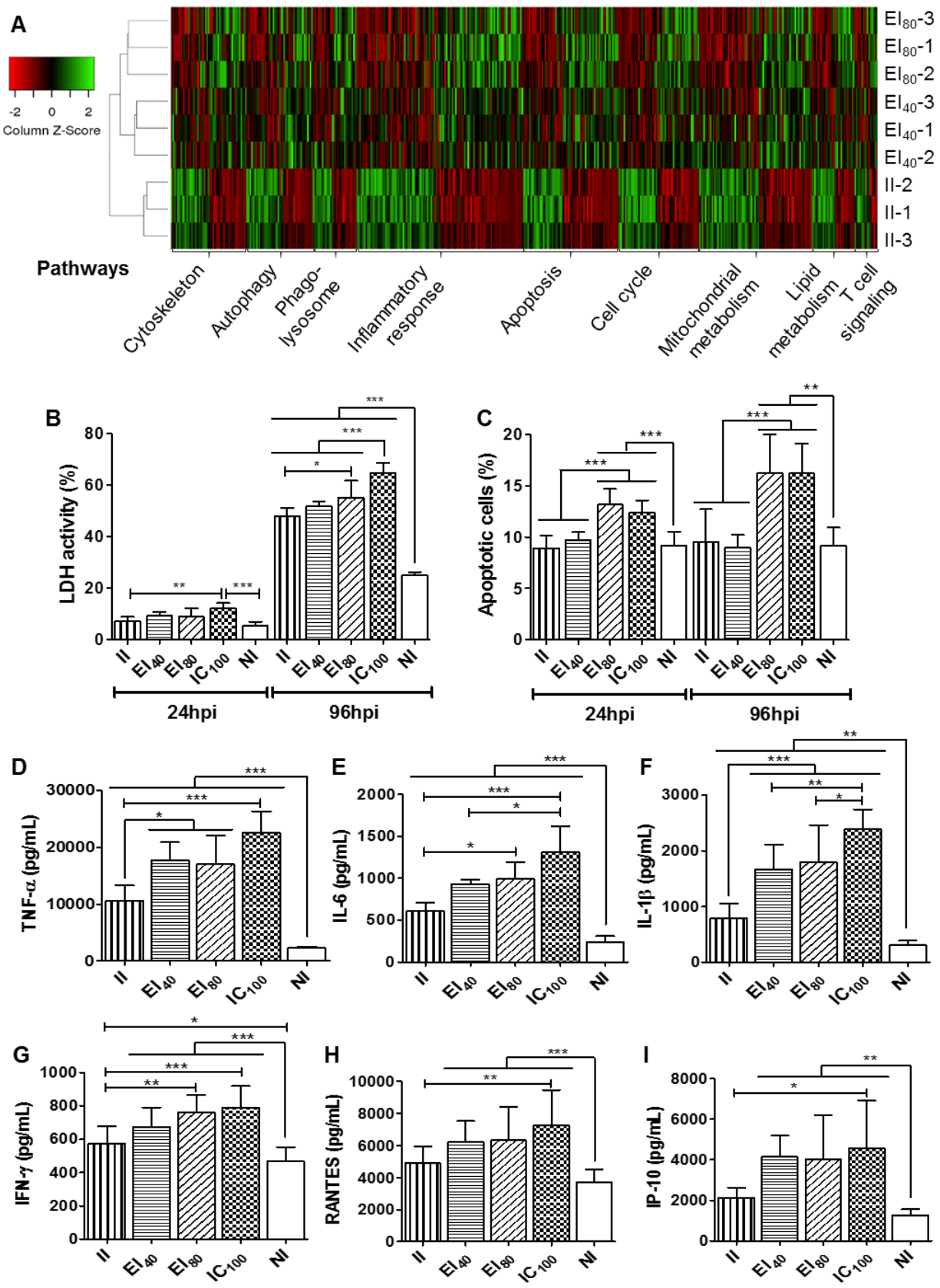

Fig. 5: Macrophage apoptosis and inflammatory response are exacerbated upon infection by isolates containing high relative frequency of the 4MBE variant.

bioRxiv preprint doi: https://doi.org/10.1101/2020.05.22.110775; this version posted May 22, 2020. The copyright holder for this preprint (which was not certified by peer review) is the author/funder. All rights reserved. No reuse allowed without permission.

Macrophages were infected at a MOI of 10:1 or not infected (NI). (**a**) At 24 hpi, total RNA were extracted to study the changes in global transcriptome of host cells. Heatmap of gene expression (log2 fold change) for 337 differentially expressed genes between II-, EI_{40}- or EI_{80}-infected macrophages at 24 hpi. Rows are independent experiments and columns are genes. Differentially expressed genes were classified in nine functional categories. Clustering was based on Pearson's correlation. The three experimental conditions clustered with their biological replicates. (**b**) Necrosis was evaluated by LDH release in cell culture supernatant and (**c**) apoptosis was measured by Annexin V staining and analysis performed by microscopy, at 24 hpi and 96 hpi. (**d**) TNF-α, (**e**) IL-6, (**f**) IL-1β, (**g**) IFN-γ, (**h**) RANTES (CCL5) and (**i**) Interferon gamma-induced protein 10 (IP-10) release in cell culture supernatant was evaluated by Luminex® Multiplex assay at 24 hpi. Values for each condition are the mean ± SD of three independent experiments. Means were compared using Repeated Measures ANOVA followed by Bonferroni test.